PAPER • OPEN ACCESS

Multifunctional-high resolution imaging plate based on hydrophilic graphene for digital pathology

View the article online for updates and enhancements.

Multifunctional-high resolution imaging plate based on hydrophilic graphene for digital pathology

Geonhee Lee[1,6]**, Yuna Oh**[2,6]**, Jung Tae Nam**[3]**, Seulgi Ji**[1]**, A-Rang Jang**[4]**, Du Won Jeong**[1]**, MinSoung Kang**[1]**, Sun Sook Lee**[1]**, Soosang Chae**[5]**, Donghwi Cho**[1] **, Jun Yeon Hwang**[3]**, Kyungeun Lee**[2,*] **and Jeong-O Lee**[1,*]

[1] Advanced Materials Division, Korea Research Institute of Chemical Technology, Gajeongro 141, Daejeon, Republic of Korea
[2] Korea Institute of Science and Technology, 5. Hwarang-ro 14-gil, Seongbuk-gu, Seoul, Republic of Korea
[3] Institute of Advanced Composite Materials, Korea Institute of Science and Technology, Jeonbuk, 55324, Republic of Korea
[4] Division of Electrical, Electronic and Control Engineering, Kongju National University, Cheonan 31080, Republic of Korea
[5] Department of Nanostructured Materials, Leibniz Institute of Polymer Research Dresden, D-01069, Dresden, Germany

E-mail: kelee@kist.re.kr and jolee@krict.re.kr

CrossMark

Abstract

In the present study, we showed that hydrophilic graphene can serve as an ideal imaging plate for biological specimens. Graphene being a single-atom-thick semi-metal with low secondary electron emission, array tomography analysis of serial sections of biological specimens on a graphene substrate showed excellent image quality with improved *z*-axis resolution, without including any conductive surface coatings. However, the hydrophobic nature of graphene makes the placement of biological specimens difficult; graphene functionalized with polydimethylsiloxane oligomer was fabricated using a simple soft lithography technique and then processed with oxygen plasma to provide hydrophilic graphene with minimal damage to graphene. High-quality scanning electron microscopy images of biological specimens free from charging effects or distortion were obtained, and the optical transparency of graphene enabled fluorescence imaging of the specimen; high-resolution correlated electron and light microscopy analysis of the specimen became possible with the hydrophilic graphene plate.

Supplementary material for this article is available online

(Some figures may appear in colour only in the online journal)

---

[6] These authors contributed equally to this work.
[*] Authors to whom any correspondence should be addressed.

1. Introduction

To study the microstructural features of cells and tissues in biological specimens, scanning electron microscopy (SEM) or transmission electron microscopy (TEM) is most often used [1, 2]. In general, in order to analyze the internal ultra-structure of a biological specimen using an electron

microscope, the specimen is hardened with a resin, and sliced into sections each 50–300 nm thick using an ultra-microtome [3]. Such ultrathin sections are handled by floating them on the surface of water and section ribbons can be collected on a TEM grid or a flat plate. In addition to general electron microscopic observations, 3D electron microscopic analyses such as array tomography can be performed using back-scattered electron (BSE)-SEM, to specifically analyze the spatial interactions in the biological specimens [4–7].

Electron microscope plates for biological specimens must meet two important criteria, especially for BSE-SEM imaging: first, the surface of the imaging plate must be hydrophilic in order to successfully mount the serial sections from an aqueous solution; and second, the plate must be somewhat electrically conductive to prevent the charging effect, an accumulation of electrons on the surface of the specimen. In general, insulating samples such as biological specimens are coated with a thin layer of metal or carbon to prevent the charging effect [8–12]. However, such post-treatments often interfere with nano-microstructures of specimens, and hence hinder the ability to make accurate observations. Recently, Kubota and colleagues demonstrated that a carbon nanotube (CNT) tape can be used as a substrate for serial-section electron microscopy of brain ultrastructures [13]. Use of a plasma-hydrophilized, CNT-coated polyethylene terephthalate tape successfully resolved the issues of section wrinkle formation and charging during imaging. However, possible artifacts arising from a CNT is envitable, since a CNT itself is curved on the nanoscale, variations in the topography of the CNT substrate on the nano-micro-scale can result in variations in the morphology and behaviors of cellular specimens [14–20]. To overcome these issues, one-atom-thick, essentially two-dimensional graphene may be considered an ideal substrate for electron microscopy imaging. The atomically smooth surface of graphene would not initiate the formation of topography-induced artifacts, and the excellent electrical conductivity of graphene would prevent sample charging during imaging. Since large-scale production of relatively uniform graphene is possible using chemical vapor deposition (CVD) [21–24] commercial production of graphene-based imaging plates is feasible [25–27]. Graphene has been used in a variety of electron microscopy imaging analysis components such as TEM grids, and as veils to image biological specimens [11]. However, there exists a problem in using graphene as an electron microscopy plate: the graphene surface is essentially hydrophobic. While the surface energy of graphene can be controlled using a substrate (due to the transparency of graphene) [28–30], it is difficult to transfer graphene onto a hydrophilic substrate. In recent years, much research has been conducted on controlling the wettability of the graphene surface through a variety of methods such as plasma treatment [27, 31, 32]. UV irradiation [33, 34], laser irradiation [34, 35], and chemical functionalization [36–40]. For example, Son *et al* used hydrogen plasma to produce hydrophilic graphene to be used as a cell substrate [31]. However, most of these methods cannot at the same time make the graphene hydrophilic and keep the graphene lattices intact and relatively free of physical and chemical

defects. Therefore, developing a technology that can easily produce hydrophilic graphene without damaging too much of its character is essential for using graphene as electron microscopy plates for biological specimens.

In the present study, we introduced polydimethylsiloxane (PDMS) oligomers onto graphene to form PDMS oligomer functionalized (PO) graphene, and subsequently, plasma was treated on the functionalized graphene surface to provide the hydrophilic, plasma-processed, PDMS oligomer functionalized (PPO) graphene. These forms of graphene were tested as electron microscopy imaging plates, and their physicochemical characteristics were investigated. Specifically, surface wettability characteristics were determined by measuring water contact angles in various conditions, surface composition analysis was achieved using x-ray photoelectron spectroscopy (XPS) and Fourier-transform infrared (FTIR) spectroscopy, and the intactness of the produced graphene was confirmed by carrying out Raman spectroscopy and sheet resistance mapping experiments. Finally, various biological specimens were prepared on imaging plates made using the produced hydrophilic graphene, and were investigated using SEM to determine the applicability of the developed procedure.

2. Results

Figure 1 shows (a) schematic of graphene imaging plate fabrication and characteristics of them. As shown in figure 1(a), PPO graphene in the present study is expected to show unique performance as an imaging plate, due to optical transparency, high electrical conductivity, and mobility, as well as secondary electron suppression characters of graphene [41–45]. Briefly, non-crosslinked PDMS oligomers diffused out from the stamp onto the graphene surfaces to provide very thin oligomer layers of ∼1 nm thick layer on graphene surfaces (FTIR spectra in figure 1(b), TEM image in figure S1 (available online at stacks.iop.org/NANO/33/505101/mmedia), and XPS spectra in figure S2) and then became hydrophilic with the plasma treatment. As shown in the figure, hydrophilic graphene imaging plates produced in the present study exhibit surface energy values suitable for placing biological specimens (see figures 1(c) and S3). Through Raman spectroscopy analyses, we have confirmed that excellent physical characteristics of graphene were relatively well-preserved; the PDMS oligomer serves to protect the graphene surface from plasma treatment (see figures S4–S6). As shown in the figure S4, though defect-related D-peak increases with plasma treatment for both oxygen plasma treated graphene and PPO graphene, PPO graphene showed larger 2D/G ratio compared to oxygen plasma-treated graphene. Also, though a significant increase in D peak has been observed with PPO graphene, D peak intensity for PPO graphene was measured to be ∼70% of that of graphene treated with oxygen plasma (figure S5). Since defects in graphene were made by plasma treatment, no D peak appeared in PO graphene (figure S6).
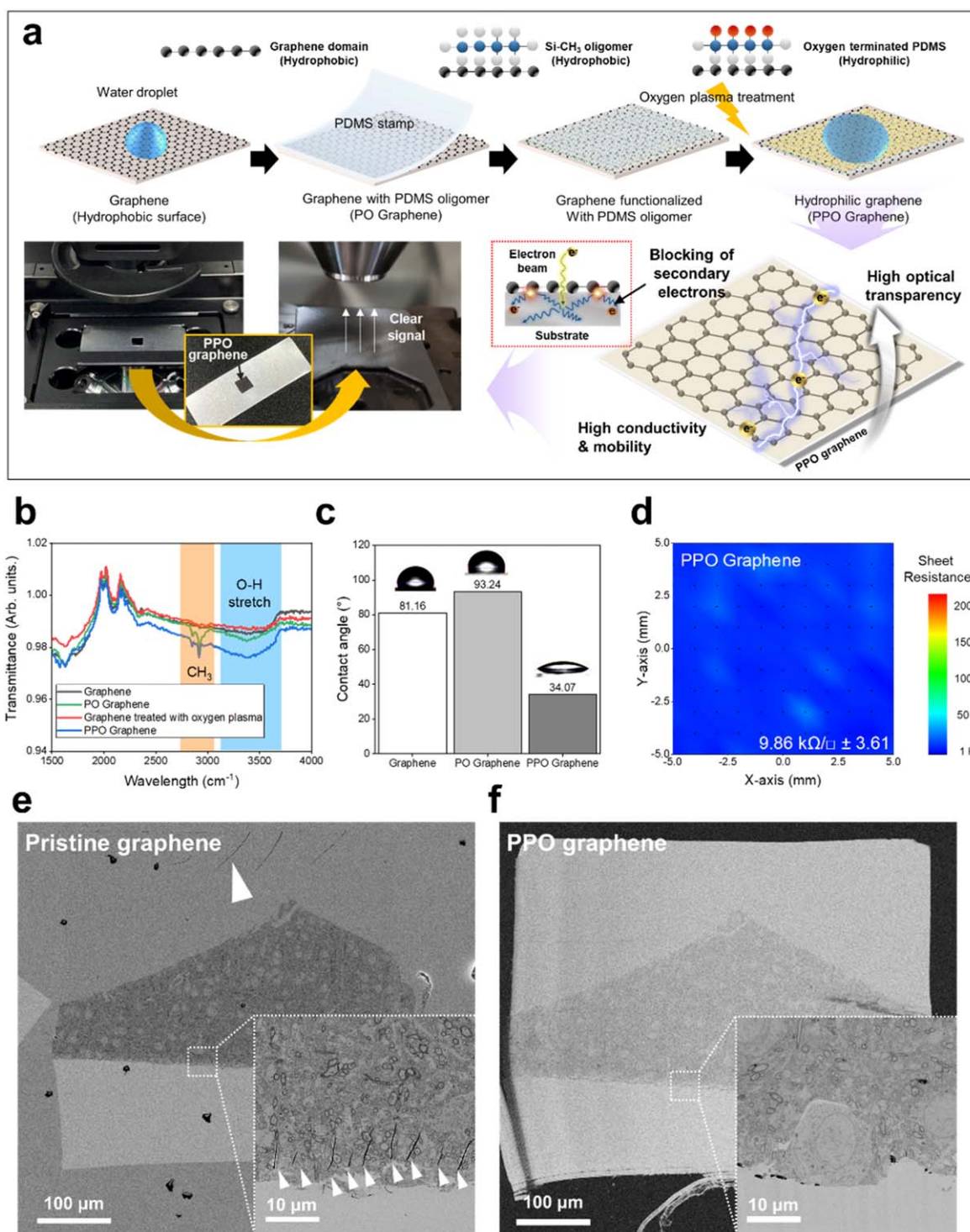
Figure 1. Fabrication and characterization of hydrophilic graphene. (a) Schematic of graphene imaging plate fabrication and unique advantage of it. (b) Fourier transform infrared spectra (FTIR) of graphene, PO graphene, graphene processed with oxygen plasma, and PPO graphene. (c) Measured water contact angles on graphene, PO graphene, and PPO graphene respectively. (d) Sheet resistance mapping images of graphene, low magnification images of section specimen placed on (e) graphene, and (f) PPO graphene. White arrowheads in e highlight wrinkles and folds on section specimen.

PPO graphene showed an average sheet resistance of 9.86 kΩ/□, which, although ∼6 times higher than that of pristine graphene, is ∼80% lower than that of the plasma-treated graphene (see figures 1(d) and S7). These results confirm the presence of PDMS oligomer layers on graphene surfaces that play a protective role against plasma irradiation and provide hydrophilic Si–OH groups. Figures 1(e) and (f) highlight the importance of surface energy of the imaging plate; while a wrinkle-free clean section specimen can be made with PPO graphene, a section specimen placed on a
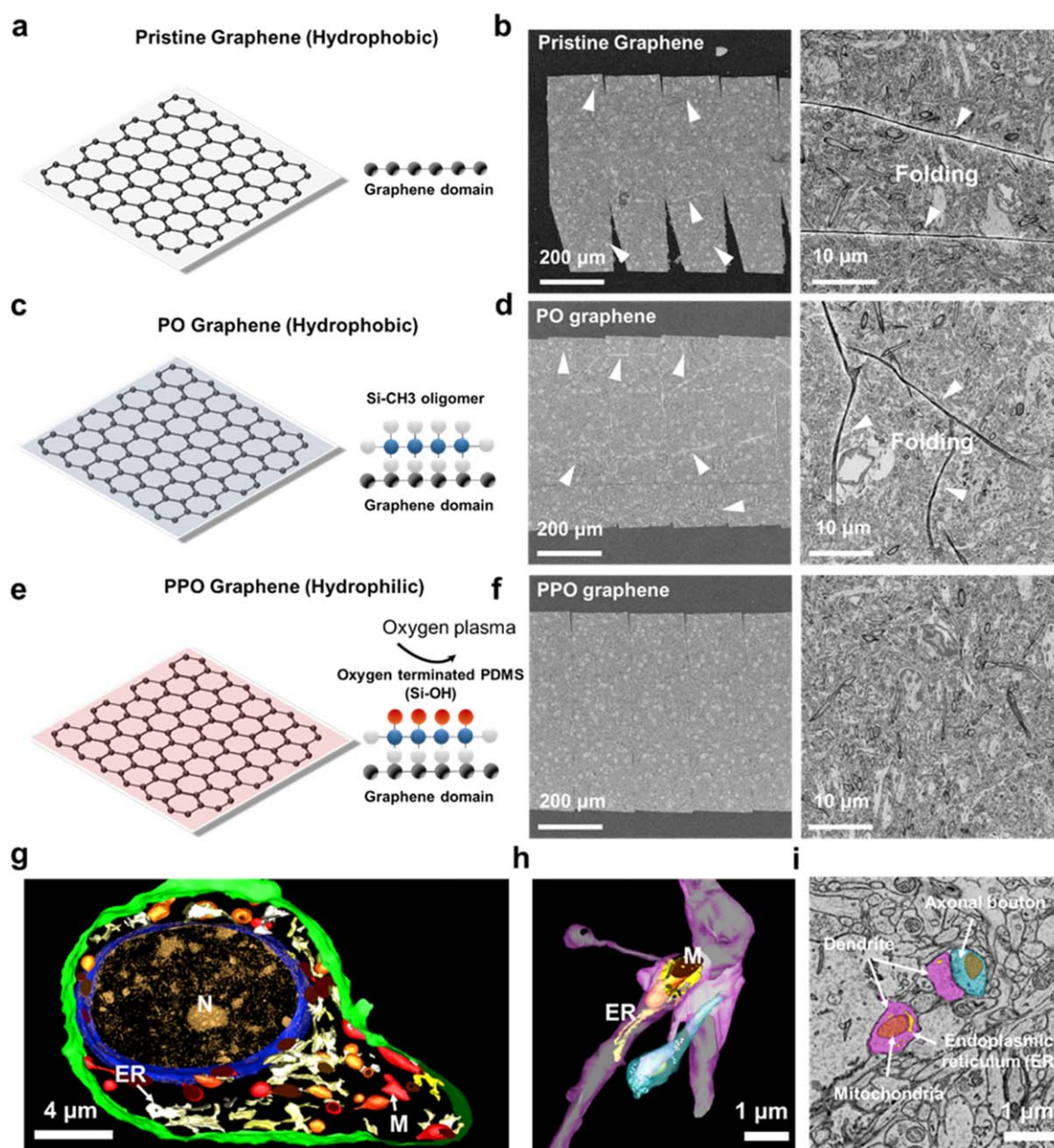
Figure 2. BSE-SEM images of serial sections and 3D reconstruction. (a)–(c) Serial sections of a mouse on (a), (b) pristine graphene, (c), (d) PO graphene, and (e), (f) PPO graphene. White arrowheads mark wrinkles in the sections. (d), (e) Representative high-magnification images of the serial sections on (d) PO graphene and e PPO graphene. 3D structures of (g) the neuronal cell body and (h), (i) dendrite and synapse, with blue showing the nucleus, green the plasma membrane of the neuronal cell body, yellow the endoplasmic reticulum (ER), red or orange the mitochondria, magenta the dendrite, sky-blue the axonal bouton, and white the synaptic vesicle.

hydrophobic, pristine graphene suffers from large amounts of wrinkles and folds.

Performances of PPO graphene imaging plate have been verified with BSE-SEM imaging of serial section specimen. Ultra-thin serial sections of specimens placed on glass slides covered with, pristine graphene, PO graphene, and PPO graphene respectively, were analyzed using BSE-SEM as shown in figure 2. We collected the serial sections that were floating on water by dipping either hydrophobic or hydrophilic flat plates into the water. As shown in figures 2(b) and (d), many wrinkles (marked with white arrowheads) were found spanning entire domains of specimens mounted on the

hydrophobic plates, i.e. those with pristine graphene and those with PO graphene. Some sections on the PO graphene (see movie M1) were observed to be deformed by the wrinkles in the high-magnification images of the same target. In contrast, as shown in figure 2(f), the specimen mounted on the hydrophilic PPO graphene plate showed no wrinkles, allowing high-resolution imaging (see movie M2). In the 3D structure reconstructed from serial images on PPO graphene (see figure 2(g) and movie M3), the subcellular organelles such as the endoplasmic reticulum (ER) and mitochondria could be clearly distinguished within the neuronal cell body. Wrinkle-free section specimens were also obtained with the
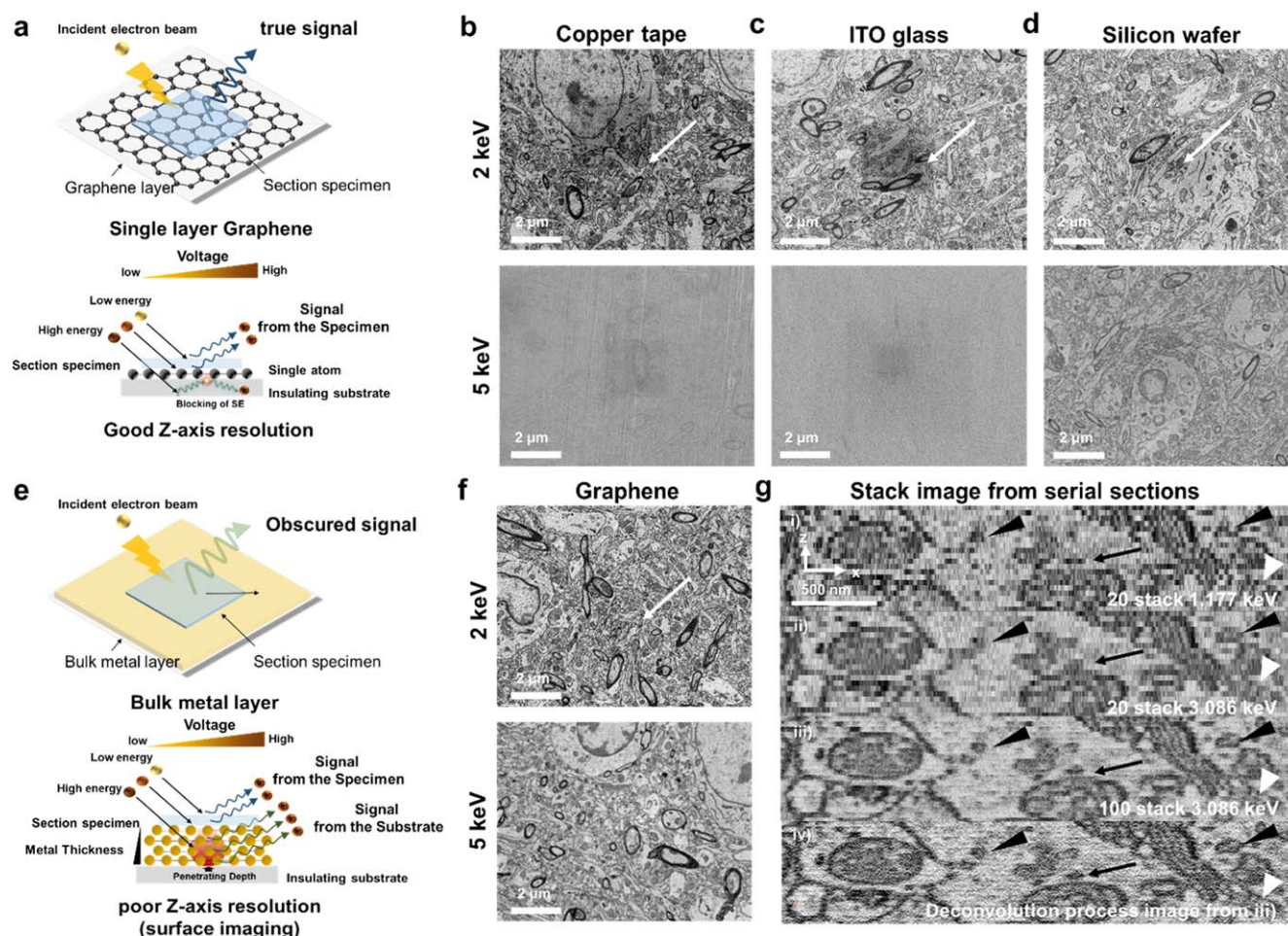
Figure 3. BSE-SEM images of ultra-thin sections on various conductive plates. (a) Schematic of multi-energy imaging with metallic substrate BSE-SEM images of ultra-thin sections on a (b) copper tape, (c) ITO glass, (d) silicon wafer and (f) graphene film. The images were acquired using acceleration voltages (AV) of 2 keV (top row) and 5 keV (bottom row). White arrows indicate in each case the focusing area. (e) Illustrates multi-energy imaging schematic with graphene plate. (f) BSE images of a representative section on PPO plate acquired with (i) 20 stacks acquired with only 1.177 keV, (ii) 20 stacks acquired with only 3.086 keV AV (iii) 100 stacks from images acquired with multi energy values of 1.177, 1.783, 2.273, 2.700 and 3.086 keV, (iv) deconvolution processed images of (iii). Black arrowheads and arrows in (g) show some vesicles and white arrowheads show the Golgi Complex.

PPO graphene substrate when we changed the section collecting method to a loop method (see figure S8), and could be used for large (2 mm wide specimens) sections as well, though a small number of wrinkles appeared on the edges of the large specimen (see figure S8(f)). Therefore, a PPO graphene substrate can be utilized to prepare wrinkle-free specimens in general BSE-SEM experiments.

Next, we investigated the importance of the electrical conductivity of the imaging plates. The imaging plate with high electrical conductivity made it possible to acquire high-resolution SEM images without conductive carbon coating process, normally used to prevent charging effect during SEM analysis (see figure S9). No significant charging effect was observed for either the pristine graphene plate or the PO graphene plate before plasma treatment was carried out (see figure S10). The inclusion of a PDMS oligomer layer on graphene treated with oxygen plasma had a marked effect on the image quality. As shown in figures S11(a) and S12(c), a severe charging effect occurred for a mouse brain section on

graphene treated with oxygen plasma (yellow arrowheads), but no charging effect was observed when using PPO graphene as the substrate (see figures S11(b) and S12(a)). Image drift and charging were also observed for plasma-treated pristine graphene films (i.e. ones without any PDMS oligomer layer) as marked with yellow arrowheads in figure S12(b).

Having a hydrophilic and electrically conductive substrate was determined, based on the above observations, we explored the advantages of graphene compared to conventional metallic substrate, which also provides excellent electrical conductivity for imaging. Figure 3(a) shows a comparison of images of mouse brain sections on various metallic or metal-like substrates including graphene-transferred glass slides. Of these tested plates, use of the graphene plate yielded the clearest images of the sectioned specimen, for both 2 keV and most notably for 5 keV acceleration voltages (AV). During BSE-SEM imaging, the penetrating depth from the surface of the section can be determined by the energy represented by the AV [46]. When higher AVs were

used, strong BSE signals and SE signals derived from the substrate with high electron density, i.e. metallic substrates, interfered and reduced the image contrast containing the structural information of the specimen (see figures 3(b)–(d)). Graphene imaging plate, however, did not cause such a problem, since graphene consisted of carbon atoms only, single-atom-thick, and known to significantly reduce secondary electron emission from the substrate [41–45]. Since the closely spaced carbon atoms (0.142 nm) in graphene enhance the elastic BSEs, fewer electrons enter below graphene, and it is even more difficult for low energy, scattered electrons to exit from graphene. Such aspects of graphene have successfully been demonstrated for suppressing secondary electron yields, which is crucial for various electronic devices including accelerators [41–45].

For three-dimensional structural analysis using serial section SEM, it is crucial to acquire images containing structural information along the entire depth of the sections; high AV that may penetrate the entire section depth has to be used. With low AV, sufficient structural information within a section cannot be obtained, because the image has gained only from the top surface of the section (see figures 3(g)–(i)). While metallic substrates including ITO exhibit obscured images with a high AV (see figure 3(c), bottom row), rich structural information could be obtained with PPO graphene by varying AV (see figure 3(f)). Therefore, PPO graphene is an ideal substrate for 3D structural analysis using serial sections. Especially, PPO graphene is irreplaceable for analyzing the 3D structures of small subcellular organelles such as ER, where thinner serial sections than subcellular organelle are needed. Multi-energy deconvolution (MED) is a method of obtaining optically sectioned images through a deconvolution process of images produced by energy-dependent penetration depth and is used to overcome the physical size limit of section specimens made using an ultramicrotome [47]. MED cannot be applied to specimens on metallic substrates due to the difficulty of imaging at high AV, nor to carbon-coated specimens on PI film, because indefinite amounts of carbon coated on the section surface obscured the penetration depth from the surface. However, with a PPO graphene imaging plate, MED analysis is possible on serial section SEM, and images with enhanced z-axis resolution can be obtained (see figures 3(g)-iv). While mitochondria and its adjacent ER could be clearly distinguished (black arrows) with a single AV, ultrastructures such as vesicles and Golgi complex could not be clearly distinguished as shown in the side view of the image stack (see figures 3(g)-i and (g)-ii). However, leaflets of Golgi complex (white arrowheads) and vesicles (black arrowheads and arrows) are clearly discernible in the side view of the image stack acquired using multi-energy and their deconvolution (see figures 3(g)-iii and (g)-iv. Dendritic ER, which is thinner than the section thickness (50 nm), is hard to reconstruct using serial section SEM analysis, can also be reconstructed in more detail from the image set containing the sub-slice images obtained using the MED method (see figure 2(g)).

Finally, unique advantages of using PPO graphene as a correlative light and electron microscopy (CLEM) plate were sought. CLEM is the combination of optical microscope (fluorescence microscope in general) and electron microscope, and is used in life science research [48]. Since the results shown by the fluorescence microscopy and the electron microscopy are different, it is intended to compensate for the shortcomings between the two methods by merging the two methods. Many fluorescent materials lose their properties during sample preparation for electron microscopy analysis. Therefore, sample preparation for CLEM is often prepared by a method with low contrast [49]. Due to the lack of any need, when using PPO graphene, to carry out a post-treatment such as surface coating (which would otherwise be necessary when imaging insulating specimens) and due to the ability to use the optical transparency of graphene, it was possible to apply dye for fluorescence microscopy and obtain both fluorescence microscopy and electron microscopy images with a single PPO graphene plate.

As a model system of CLEM using PPO graphene, intra-cellular distribution of fluorescence-labeled cell penetration peptide (CPP) has been investigated. Figures 4(a) and (b) show fluorescence images and corresponding BSE-SEM images of serial sections respectively. Here, the ultrathin serial sections of TAMRA (red) labeled CPP treated cells after CLEM sampling were placed on a PPO graphene plate and then stained using DAPI reagent (Fixed Cell ReadyProbesTM Reagent DAPI). Since we could not observe the cellular membrane with the fluorescent microscope, and the CPPs appeared not far from the nucleus as shown in the high-resolution fluorescence microscope images in figure 4(a)-(i), the presumed location of CPPs was in the cytoplasm. However, as shown in the CLEM images in figure 4(c), CPPs were located inside the vesicles that were released out of the cell. 3D rendered images of CLEM in figures 4(d), (e) also confirmed overall distribution of CPPs in vesicles situated outside of the cell. Therefore, functional analysis of biological systems with highly improved 3D spatial resolution is possible with the PPO graphene in the present study. Although conductive ITO thin films were used for CLEM previously [50], those are no match for PPO graphene. High AV, which is necessary for improved z-axis resolution cannot be used due to charging effect and secondary electrons coming from the ITO plate. It is also worth mentioning that ITO plates used for CLEM previously had higher electrical conductivity than monolayer graphene used in the present study. Presumably, the excellent charge mobility of graphene enabled efficient redistribution of back-scattered electrons to prevent charging effect [51]. In addition, as shown in figure S13, the fluorescence microscopy images of section specimens placed on ITO plates showed inferior image quality to PPO graphene, confirming the superiority of PPO graphene in CLEM imaging.

We expect that continued work on CLEM analysis will contribute to a better understanding of biological specimens, and we plan to develop a protocol for bimodal, CLEM image analysis of biological specimens using the PPO graphene imaging plate in the present study.
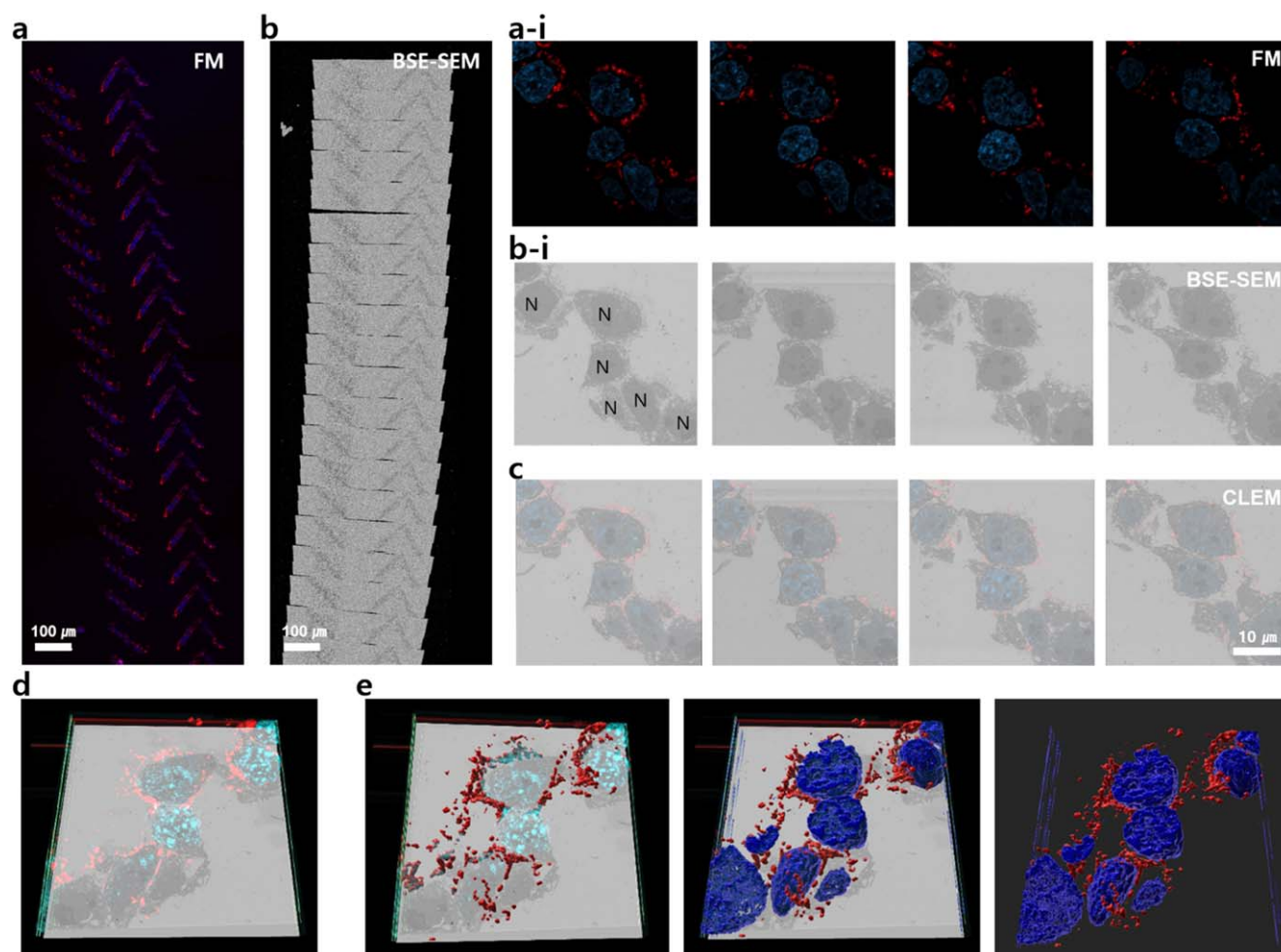
Figure 4. Correlative light and electron microscopic (CLEM) analysis of culture cell on a PPO graphene plate. (a) Low magnified fluorescent image of serial sections from culture cell and (a)-(i) higher magnified representative fluorescence images, (b) Low magnified BSE-SEM image of serial section and (b)-(i) higher magnified BSE-SEM images of the same sections. (c) Merged fluorescence/SEM images. N; nucleus. DAPI stained regions (blue) were matched well with nucleus structures in BSE-SEM images, (d) the stacked fluorescence images with a representative BSE-SEM image, (e) 3D rendering images of the stacked fluorescence images. The serial fluorescent images are well aligned and show the three-dimensional distribution of CPPs. A movie showing rendered 3D images is shown in the supplementary information movie M4.

3. Conclusion

In summary, we demonstrated plasma-treated, PDMS oligomer-functionalized graphene (PPO graphene) as a multifunctional imaging plate for biological specimens. PDMS oligomer layers that diffused onto graphene surfaces as a result of PDMS stamping for 30 min protected the graphene from oxygen plasma treatment and at the same time made the surface hydrophilic. Such prepared plates were effective even for large sections of biological specimens; the hydrophilicity of the plates prevented specimen sections from forming wrinkles or folds, and no charging or image distortions occurred because the excellent electrical properties of graphene were maintained due to the protection afforded by the PDMS oligomer layer. While specimen sections on metallic substrates such as Cu or ITO cannot be properly imaged with high voltage due to the high density of BSE signals coming from the substrate, in contrast, graphene—being a single layer of carbon atoms arranged in a two-dimensional honeycomb lattice—is free of such issues since the subject specimen is mainly composed of carbon just as is graphene/polymer, and therefore can be considered to be an ideal substrate for BSE-SEM analysis. These unique characteristics of graphene enabled its deployment in our experiments to improve the *z*-resolution using MED electron microscopy. Moreover, the optical transparency of graphene combined with its high electrical conductivity enabled a bimodal (confocal fluorescence microscopy and electron microscopy) analysis of a biological specimen with a single plate. The imaging plate in the present study can be commercialized at an affordable price, as the plates can be produced on various plastic substrates as shown in figure S14. Yet, scalable production and processing of graphene, as well as expansion of applications of the imaging plate needs to be preceded. Considering that the properties shown in the present study (optical transparency, electrical conductivity, and excellent charge mobility with a truly two-dimensional electron density distribution) are only possible with graphene, and considering the simplicity of

producing the hydrophilic graphene plate used in the present study, this plate may become the first commercial product of any type to use the unique advantages of graphene [52].

4. Experimental section

4.1. Preparation of graphene films on glass

Graphene grown on a Cu foil was purchased from MCK Tech Co., Ltd. (Daejeon, Korea). A solution of poly(methyl methacrylate) (PMMA C4, 4% by volume dissolved in chlorobenzene) (Microchem, USA) was spin-coated onto the top surface of a graphene/Cu foil at 500 rpm for 10 s and 2000 rpm for 30 s. Then, the PMMA/graphene/Cu foil was baked at 80 °C for 5 min. The Cu foil under PMMA/graphene was etched by using a CE-100 copper etchant solution (Transene Inc., Danvers, MA, USA). After etching the Cu foil, the PMMA/graphene layer was washed with deionized water (DI-water) three times, for 1 h each time. Finally, the PMMA film on the graphene/glass was dipped in an acetone solution for 3 h and then washed with isopropyl alcohol (IPA) three times to remove the PMMA film. Most graphene imaging plates were made on glass slides unless otherwise noted.

4.2. Surface modification for producing hydrophilic graphene

To transfer PDMS oligomer onto graphene, a PDMS stamp was fabricated using a Silicone Elastomer Kit (Sylgard 184, Dow Corning, USA). Silicone elastomer base and curing agent were mixed at a 10:1 (v/v) ratio and poured into a square petri dish. The PDMS mixture was degassed and then followed by curing at 70 °C for 4 h and releasing from the petri dish. Fabrication of the PDMS stamp for oligomer transfer was completed by cutting the released cured material to fit the sample size for surface treatment. Then, the prepared PDMS stamp was gently attached to the surface of graphene on a glass substrate for 30 min. After removing the PDMS stamp from the graphene surface, PDMS-oligomer-engineered graphene on glass was placed in a plasma system (200LF plasma processing system, Femto Science, KOREA) and treated with oxygen plasma with 80 W power for a duration of 10 s. Water contact angles were measured at various PDMS stamping times, including 5 min, 10 min, and 30 min of stamping as well as longer, on a glass substrate and graphene/glass (see figure S3) to find optimum conditions. The PDMS oligomer layers on graphene were observed to be very stable in ambient conditions, as shown in figure S15, but after the plasma treatment, the water contact angle of hydrophilic graphene gradually increased to ~65° after three days of being stored at room temperature (figure S16).

4.3. Characterizations

Chemical binding analyses of PDMS oligomer/graphene were conducted by XPS (K-Alpha instrument, Thermo Scientific, USA) with the incident beam produced by an Al x-ray source ($h\nu = 1486.6$ eV) and a pass energy of 50 eV. Sheet resistance mappings of functionalized graphene were obtained using a four-probe technique (CMT- SR1000N, Advanced Instrument Technology, USA). Changes in the functional groups of the PDMS oligomer layer were monitored using FTIR spectroscopy (Bruker ALPHA-P, USA), and surface topography information was obtained with atomic force microscopy (AFM, Digital Instruments Dimension 3000, Veeco Science, USA) in tapping mode. Raman spectrum analysis was carried out with a Raman microscope (inVia™, Renishaw, UK). Raman mapping images were obtained from 196 spectra (a 30 μm $\times$ 30 μm area). The interval between consecutive spectrum points was 1.5 μm horizontally and vertically.

4.4. Sample preparation for BSE-SEM

Samples were prepared using the reduced osmium-TCH-osmium (ROTO) staining method. Pre-fixation was performed with 2.5% glutaraldehyde in 0.1 M cacodylate buffer. Fixed samples were washed with 0.1 M cacodylate buffer. Post-fixation steps were then sequentially carried out and involved incubations in reduced osmium (2% osmium tetroxide and 1.5% potassium ferrocyanide) solution, 1% thiocarbohydrazide solution, and 2% osmium tetroxide solution. En bloc staining was performed sequentially using 1% uranyl acetate aqueous solution and lead aspartate solution. After washing, samples were dehydrated gradually (30%, 50%, 70%, 80%, 90%, and 100%) for resin embedding. Samples were embedded in Spurr's resin (60 °C for 24−48 h).

4.5. Sample preparation for CLEM

Samples sectioned using an ultramicrotome (MT XL microtome, RMC Boeckeler, USA) were placed on plates. Pre-treated biological specimens as in the Experimental section 2.4 were thinly sliced into sections each with a thickness of 50–100 nm using an ultramicrotome for SEM observations and placed on plates. To transfer the sliced sections onto the imaging plates, either a loop or substrate holder (ASH2, RMC Boeckeler, USA) was used, though the loop method was the preferred one. The serial sections were obtained using the substrate holder (ASH2). Samples obtained using the above procedure were observed using SEM (Teneo versus, FEI, installed in KIST). SEM images were taken at a working distance of about 4 mm, with 2 keV AV and 0.1 nA emission current, in back-scattered electron (BSE) detector mode.

4.6. SEM observations

Resin-embedded biological samples were thinly sliced into sections each with a thickness of 50–100 nm by using an ultramicrotome (MT XL microtome, RMC Boeckeler, USA) and placed on plates for SEM observations. To transfer the sliced sections onto the imaging plates, either a loop or substrate holder (ASH2, RMC Boeckeler, USA) was used. The transferred sections were observed using SEM (Teneo versus, FEI, USA). Tiles in a 2 $\times$ 2 arrangement, with each tile having dimensions of 4096 pixels $\times$ 4096 pixels, were used at a working distance of about 4 mm, with a 2 keV AV and 0.1 nA emission current, in a T1 detector with a 5 nm pixel size,

and stitched using MAPS Array tomography software (FEI). For 3D reconstruction, IMOD software was used [53]. For applying the MED technique, SEM images of 20 serial sections were taken with 1.177 keV, 1.783 keV, 2.273 keV, 2.7 keV, and 3.086 keV AV and a 0.1 nA emission current, in a T1 detector using the MAPS versus mode.

4.7. CLEM observations

Resin-embedded CLEM sample was thinly sliced into sections with a thickness of 50 nm by using an ultra-microtome (MT XL microtome, RMC Boeckeler, USA) and transferred onto the PPO imaging plates using a substrate holder (ASH2, RMC Boeckeler, USA). The sections were observed using a confocal microscope (LSM800, ZEISS, Germany) and SEM (Teneo versus, FEI, USA).

4.8. Cross-sectional sample preparation for TEM imaging

Cross-sectional TEM specimens were prepared using focused ion beam (FIB) milling for graphene and PDMS oligomer/graphene samples as shown in Supplementary materials figure S1. To prevent the surfaces of the samples (graphene and the oligomer-treated graphene) from becoming damaged, each of these samples was coated with a Pt film was coated during the FIB process. Sequentially, samples were milled with a Ga ion beam to make the section thickness less than a few micrometers, and then specific sites of the samples were lifted out to be attached to the TEM specimen grid. The fixed section was milled again with a Ga ion beam to have a thin section less than 100 nm thick. Thin sections obtained through the above procedure were observed by TEM (Titan Cubed G2, FEI, USA), with 80 keV accelerating voltages.

Data availability statement

All data that support the findings of this study are included within the article (and any supplementary files).

Conflict of interest

There are no conflict to declare.

ORCID iDs

Donghwi Cho ⬤ https://orcid.org/0000-0001-9382-3820
Jeong-O Lee ⬤ https://orcid.org/0000-0002-7343-4892

References

[1] Midgley P A, Ward E P W, Hungría A B and Thomas J M 2007 *Chem. Soc. Rev.* **36** 1477–94

[2] Marsh B J, Mastronarde D N, Buttle K F, Howell K E and McIntosh J R 2001 *Proc. Natl. Acad. Sci. USA* **98** 2399–406

[3] De Jonge N, Peckys D B, Kremers G J and Piston D W 2009 Electron microscopy of whole cells in liquid with nanometer resolution *Proc. Natl. Acad. Sci. USA* **106** 2159–64

[4] Alberts B, Johnson A, Lewis J, Raff M, Roberts K and Walter P 2002 *Molecular Biology of the Cell* 4th edn

[5] Micheva K D and Smith S J 2007 *Neuron* **55** 25–36

[6] Burel A *et al* 2018 *Development* **145** dev160879

[7] Hayworth K J *et al* 2014 *Front. Neural Circuits* **8** 1–18

[8] Muscariello L *et al* 2005 *J. Cell. Physiol.* **205** 328–34

[9] Stokroos I, Kalicharan D, Van Der Want J J L and Jongebloed W L 1998 *J. Microsc.* **189** 79–89

[10] Golding C G, Lamboo L L, Beniac D R and Booth T F 2016 *Sci. Rep.* **6** 1–8

[11] Koo K, Dae K S, Hahn Y K and Yuk J M 2020 *Nano Lett.* **20** 4708–13

[12] Park J B *et al* 2016 *2D Mater.* **3** 045004

[13] Kubota Y *et al* 2018 *Nat. Commun.* **9** 1–3

[14] Lee K *et al* 2016 *J. Nanobiotechnol.* **14** 1–10

[15] Sunami H, Yokota I and Igarashi Y 2014 *Biomater. Sci.* **2** 399–409

[16] Kim J *et al* 2015 *Acta Biomater.* **27** 13–20

[17] Salaita K *et al* 2010 *Science* **327** 1380–5

[18] Abagnale G *et al* 2017 *Stem Cell Rep.* **9** 654–66

[19] Krishna L *et al* 2016 *Stem Cell Res. Ther.* **7** 1–12

[20] Cai N *et al* 2010 *ACS Appl. Mater. Interfaces* **2** 1038–47

[21] Lin L *et al* 2019 *Nat. Commun.* **10** 1–7

[22] Bae S *et al* 2010 *Nat. Nanotechnol.* **5** 574–8

[23] Deng B, Liu Z and Peng H 2019 *Adv. Mater.* **31** 1800996

[24] Lee G *et al* 2019 *Carbon* **141** 774–81

[25] Pantelic R S *et al* 2011 *J. Struct. Biol.* **174** 234–8

[26] Russo C J and Passmore L A 2016 *Curr. Opin. Struct. Biol.* **37** 81–9

[27] Russo C J and Passmore L A 2014 *Nat. Methods* **11** 649–52

[28] Raj R, Maroo S C and Wang E N 2013 *Nano Lett.* **13** 1509–15

[29] Kong W *et al* 2018 *Nat. Mater.* **17** 999–1004

[30] Chae S *et al* 2017 *Nano Lett.* **17** 1711–8

[31] Son J *et al* 2020 *Nano Lett.* **20** 5625–2631

[32] Yang J, Zhang Z, Men X, Xu X and Zhu X 2010 *Langmuir* **26** 10198–202

[33] Xu Z, Ao Z, Chu D, Younis A, Li C M and Li S 2014 *Sci. Rep.* **4** 6450

[34] Nasser J, Lin J, Zhang L and Sodano H A 2020 *Carbon* **162** 570–8

[35] Li Y *et al* 2017 *Adv. Mater.* **29** 1700496

[36] Rafiee J, Rafiee M A, Yu Z Z and Koratkar N 2010 *Adv. Mater.* **22** 2151–4

[37] Dong J, Yao Z, Yang T, Jiang L and Shen C 2013 *Sci. Rep.* **3** 1733

[38] Ostrowski J H J and Eaves J D 2014 *J. Phys. Chem. B* **118** 530–6

[39] Ashraf A *et al* 2016 *Nano Lett.* **16** 4708–12

[40] Hong G, Han Y, Schutzius T M, Wang Y, Pan Y, Hu M, Jie J, Sharma C S, Müller U and Poulikakos D 2016 *Nano Lett.* **16** 4447–53

[41] Aguincha R *et al* 2020 *Appl. Surf. Sci.* **504** 143870

[42] Nguyen H K A, Mankowski J, Dickens J C, Neuber A A and Joshi R P 2018 *AIP Adv.* **8** 015325

[43] Cao M, Zhang X S, Liu W H, Wang H G and Li Y D 2017 *Diam. Relat. Mater.* **73** 199–203

[44] Shihommatsu K, Takahashi J, Momiuchi Y, Hoshi Y, Kato H and Homma Y 2017 *ACS Omega* **2** 7831–6

[45] Luo J *et al* 2011 *ACS Nano* **5** 1047–55

[46] He Q, Hsueh M, Zhang G, Joy D C and Leapman R D 2018 *Sci. Rep.* **8** 12985

[47] De Goede M, Johlin E, Sciacca B, Boughorbel F and Garnett E C 2017 *Nanoscale* **9** 684–9

[48] De Boer P, Hoogenboom J P and Giepmans B N G 2015 *Nat. Methods* **12** 503–13

[49] Kim D, Deerinck T J, Sigal Y M, Babcock H P, Ellisman M H and Zhuang X 2015 *PLoS One* **10** e0124581

[50] Pluk H, Stokes D J, Lich B, Wieginga B and Fransen J 2009 *J. Microsc.* **233** 353–63

[51] Crawford G P 2005 Flexible Flat Panel Display Technology *Flex. Flat Panel Displays* (Wiley) ch 1 1–9

[52] Kong W *et al* 2019 *Nat. Nanotechnol.* **14** 927–38

[53] Kremer J R, Mastronarde D N and McIntosh J R 1996 *J. Struct. Biol.* **116** 71–6